Available online at www.sciencedirect.com
ScienceDirect
Trans. Nonferrous Met. Soc. China 29(2019) 515−525
Transactions of Nonferrous Metals Society of China
www.tnmsc.cn

# Microstructure and mechanical properties of as-cast and extruded biomedical Mg−Zn−Y−Zr−Ca alloy at different temperatures

Qing-gong JIA[1,2], Wen-xin ZHANG[1,2], Yi SUN[1,2], Chun-xiang XU[1,2], Jin-shan ZHANG[1,2], Jun KUAN[1,2]

1. College of Materials Science and Engineering, Taiyuan University of Technology, Taiyuan 030024, China;
2. Shanxi Key Laboratory of Advanced Magnesium-based Materials, Taiyuan 030024, China

Received 10 March 2018; accepted 12 November 2018

**Abstract:** A type of biomedical magnesium alloy Mg−3Zn−1Y−0.6Zr−0.5Ca was cast and extruded at three extrusion temperatures of 270, 300 and 330 °C. The microstructure and mechanical properties of the cast and extruded alloys, tailored at different extrusion parameters, were investigated using tensile tests, optical microscopy, scanning electron microscopy, energy dispersive spectroscopy, X-ray diffractometry, transmission electron microscopy and electron backscattered diffraction. Optimum comprehensive mechanical properties are achieved in the alloy extruded at 270 °C, the ultimate tensile strength and the elongation reach 315 MPa and 26%, respectively, which is deemed to be associated with the grain refinement, weak basal texture and second phases strengthening. After hot extrusion, extensive dynamic recrystallization is found in the Mg−3Zn−1Y−0.6Zr−0.5Ca alloy. Continuous $Mg_3YZn_6$ phase bands are gradually broken into discontinuous chain-like or dot-like structures, and the grains distribute more uniformly. The as-extruded Mg−3Zn−1Y−0.6Zr−0.5Ca alloy exhibits a weak texture with (0001) basal planes parallel to the extrusion direction.
**Key words:** magnesium alloy; quasicrystal; hot extrusion; dynamic recrystallization; mechanical properties

## 1 Introduction

Magnesium alloys have been extensively applied in the fields of bone implants, bone tissue engineering scaffolds and cardiovascular stents because of their excellent properties, such as high specific strength and rigidity, biodegradation and biocompatibility, low density (1.74−2.0 g/cm$^3$) and elastic modulus (41−45 GPa) to avoid stress shielding [1−4]. However, magnesium alloys as biodegradable implant materials also have disadvantages, including low strength and poor corrosion resistance in biological systems, which limit their clinical application. Especially, magnesium intrinsic strength cannot be maintained because of the process of human body degradation [5−7]. Therefore, it is necessary to improve the comprehensive mechanical properties of biomedical magnesium alloys.

Hot extrusion has a critical influence on the mechanical properties of the magnesium alloys and is widely investigated by many researchers [8−11]. Extrusion can effectively refine the grain size, affect the texture types and improve the strength and ductility [12−14]. SUN et al [15] systematically investigated the effect of extrusion on precipitation, microstructure and mechanical properties of Mg−4.0Zn−0.2Ca alloy, and the results are consistent with the above explanation. In recent years, fine-grained Mg−Zn−Y alloy systems reinforced by quasicrystalline *I*-particles have been successfully prepared by thermomechanical processes such as hot extrusion [16−18]. Quasicrystal *I*-phase has high hardness, good thermal stability, high corrosion resistance and low interfacial energy [19]. Besides, *I*-phase particles are stable against coarsening and can effectively impede the slip of dislocations during hot deformation [20−22]. In addition to the icosahedral quasicrystal *I*-phase, some second phases are also present in the Mg−Zn−Y alloys, such as 14H and 18R long period stacking ordered phase [23]. Although these types of alloy systems have high strength, more rare earth element Y is added to the alloys. These alloys increase costs and are not suitable for biomedical application.

The current investigation based on the Mg−Zn−Y alloys mainly focused on extrusion deformation. Although the alloys showed high strength after extrusion, low elongation or inappropriate alloy composition design

**Foundation item:** Projects (51574175, 51474153) supported by the National Natural Science Foundation of China
**Corresponding author:** Chun-xiang XU; E-mail: xuchunxiang2012@126.com
DOI: 10.1016/S1003-6326(19)64960-5

restricted their biomedical application. It is well-known that temperature is generally one of most important factors during hot extrusion [24,25]. It can control the final microstructure and texture evolution, leading to optimum mechanical properties. Accordingly, a low cost biomedical Mg−3Zn−1Y−0.6Zr−0.5Ca alloy with high plasticity was designed in this study. In addition, the relationship among extrusion temperature, microstructure and mechanical properties for as-cast and as-extruded alloys was systematically investigated.

## 2 Experimental

The experimental alloys were melted by using high-purity Mg, Zn, Y, Mg−30%Zr and Mg−30%Ca master alloys in an electric resistance furnace under the protection of anti-oxidizing gas atmosphere (1 vol.% $SF_6$ + 99 vol.% $CO_2$). All materials were preheated to 200 °C to remove the moisture from the surface. The preheated Zn was added into the melt at 700 °C after the melting of pure Mg. Then, Y and Mg−Zr master alloys were added into the melt in sequence when the temperature reached 750 °C, and held for 30 min. Subsequently, the Mg−Ca master alloys were added into the melt at 740 °C and held for 20 min. After being cooled to 730 °C, the melts were poured into a steel mold preheated at 200 °C. Then, the ingot was performed by homogenizing at 400 °C for 24 h in a vacuum tube furnace. At last, the ingot was quenched with water as quickly as possible. The as-homogenized ingot was machined into rods with a diameter of 40 mm and a length of 50 mm. Then, these rod-shaped ingots were extruded at different temperatures (270, 300 and 330 °C) with the extrusion ratio of 16:1 at a constant ram speed of 1 mm/s. Finally, the extruded bars with a diameter of 10 mm were obtained.

Phase constitution analyses were performed with Y−2000 X-ray diffractometer (XRD) using mono-chromatic Cu $K_\alpha$ radiation. The microstructures and compositions of different phases of the alloys were investigated by optical microscopy (OM), scanning electron microscopy (SEM, TESCAN-MIRA3) equipped with energy dispersive spectroscopy (EDS), transmission electron microscopy (TEM, JEOL 2010) and electron backscattered diffraction (EBSD). The average grain size and volume fraction of DRXed grains were measured by Image-Pro Plus 6.0 software. Thin foils for TEM observation were prepared by cutting the bulk sample into slices, grinding to the thickness of about 50 μm, and ion milling finally. EBSD samples were initially ground by emery papers, and then followed by electro-polished with a solution of 60 mL orthophosphoric acid together with 100 mL ethanol at room temperature and electric current of 0.2−0.5 A for 30−80 s. Tensile specimens were performed by a DNS100 electronic universal material test machine with a crosshead speed of 0.2 mm/min at ambient temperature. The sketch map and dimensions of the tensile specimens are shown in Fig. 1, with a gage dimension of 18 mm × 4 mm × 2 mm. All the tensile specimens were obtained parallel to the extrusion direction.

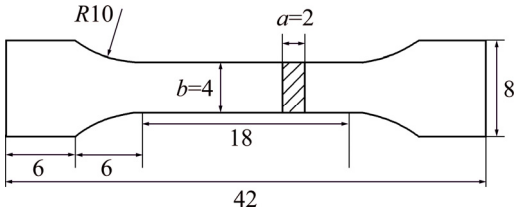


**Fig. 1** Sketch map and dimensions of tensile specimen (unit: mm)

## 3 Results and discussion

### 3.1 Microstructure

Figure 2 depicts the OM and SEM images of the as-cast Mg−3Zn−1Y−0.6Zr−0.5Ca alloys. It is shown that the as-cast alloy consists of almost equiaxed grains and the second phase in a shape of semi-continuous networks. The average grain size of the as-cast alloy is approximately 80 μm. Precipitates are not only distributed along the grain boundaries but also within the grain interior. From the magnified SEM image (Figs. 2(c) and (d)), it can be seen that precipitates mainly show the long strip-like and dot-like structures. Indentification of different second phases was carried out by XRD and confirmed by EDS results. Combined with the EDS results (Table 1), the $MgZn_2$ phases in as-cast alloy mainly exhibit a spherical structure, and distribute within the grains. Some also attach along grain boundaries, as shown in Fig. 2(c). The *I*-phase ($Mg_3YZn_6$) tends to form at the triple junctions of grain boundaries and displays a strip-like structure, as shown in Fig. 2(d).

*I*-phase is identified by TEM image and selected area electron diffraction (SAED), as shown in Fig. 3. The SAED patterns taken from the eutectic lamellar phase show the typical 3-fold and mirror fold symmetries, respectively, which are distinctive characteristics of *I*-phase. Meanwhile, it can be clearly seen from the bright-field image that *I*-phase shows a typical lamellar structure, which is consistent with the morphology of the *I*-phase of the above analysis.

Figure 4 shows XRD patterns of the as-cast alloy and as-extruded alloys at different temperatures. The as-cast alloy is primarily composed of $\alpha$-Mg, $MgZn_2$ and $Mg_3YZn_6$ phases. The absence of the Ca-containing phase in the alloy is probably ascribed to the relatively small amount of Ca. After extrusion, the phase compositions of the samples are not changed, suggesting

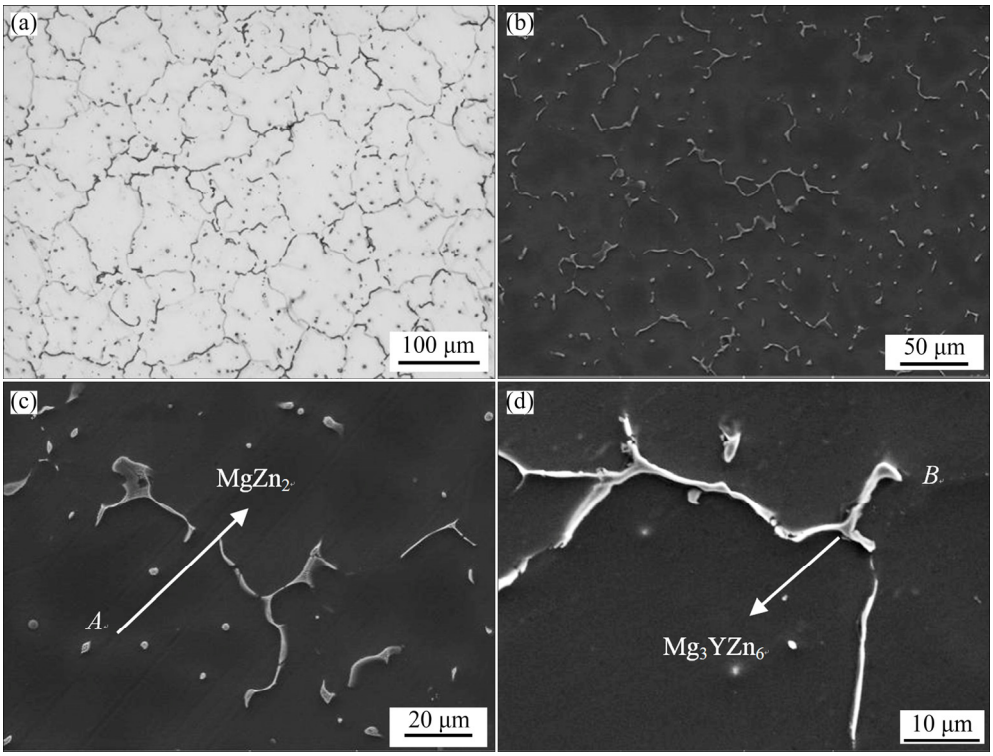


**Fig. 2** OM (a) and SEM (b−d) images of as-cast Mg−3Zn−1Y−0.6Zr−0.5Ca alloy

**Table 1** EDS results of phases at Point *A* in Fig. 2(c) and Point *B* in Fig. 2(d)

| Point | Content/at.% | | | | | Possible phase |
|---|---|---|---|---|---|---|
| | Mg | Zn | Y | Zr | Ca | |
| *A* | 34.6 | 63.6 | 1.8 | − | − | $MgZn_2$ |
| *B* | 57.0 | 29.4 | 11.4 | 1.5 | 0.7 | $Mg_3YZn_6$ |

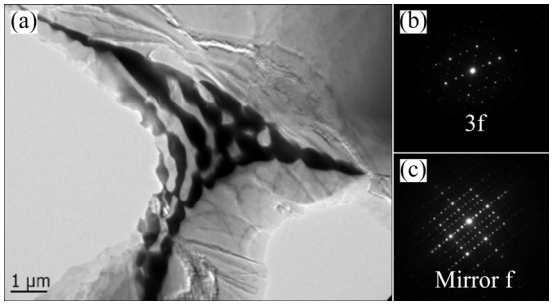


**Fig. 3** TEM BF image (a) and corresponding SAED patterns (b, c) of quasicrystal *I*-phase in as-cast alloy

that hot extrusion could not lead to the phase transformation [26]. However, the intensity of the peak located at 2$\theta$ around 34.5° is very strong compared with that of the as-cast alloy, which means that the majority of the $\alpha$-Mg grains are basically parallel to the extrusion direction [27].

Figure 5 shows the OM microstructures and average grain size of Mg−3Zn−1Y−0.6Zr−0.5Ca alloys extruded at different temperatures. Compared with the as-cast

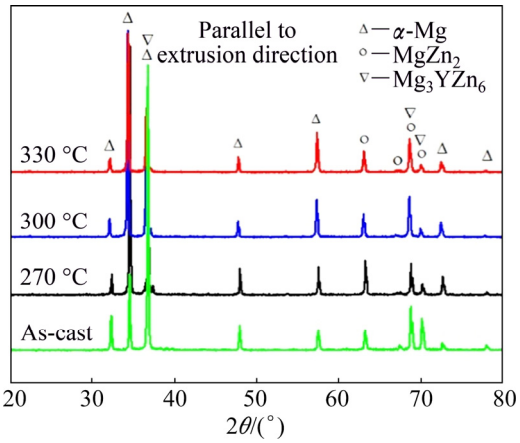


**Fig. 4** XRD patterns of as-cast and as-extruded alloys at different temperatures

alloy, the grain size of extruded alloys decreases significantly because of the occurrence of dynamic recrystallization (DRX). According to the EBSD analysis, the average grain sizes are 1.52, 2.26 and 2.64 μm at extrusion temperatures of 270, 300 and 330 °C, respectively. It is revealed that the higher the extrusion temperature, the larger the grain size of the alloy. Meanwhile, the volume fraction of DRXed grains increases from 87.2% to 94.7% with the increase of extrusion temperature from 270 to 330 °C, suggesting that the increase of temperature is helpful for the process of recrystallization. In fact, the grain size of the extruded alloy is very sensitive to the extrusion temperature. As

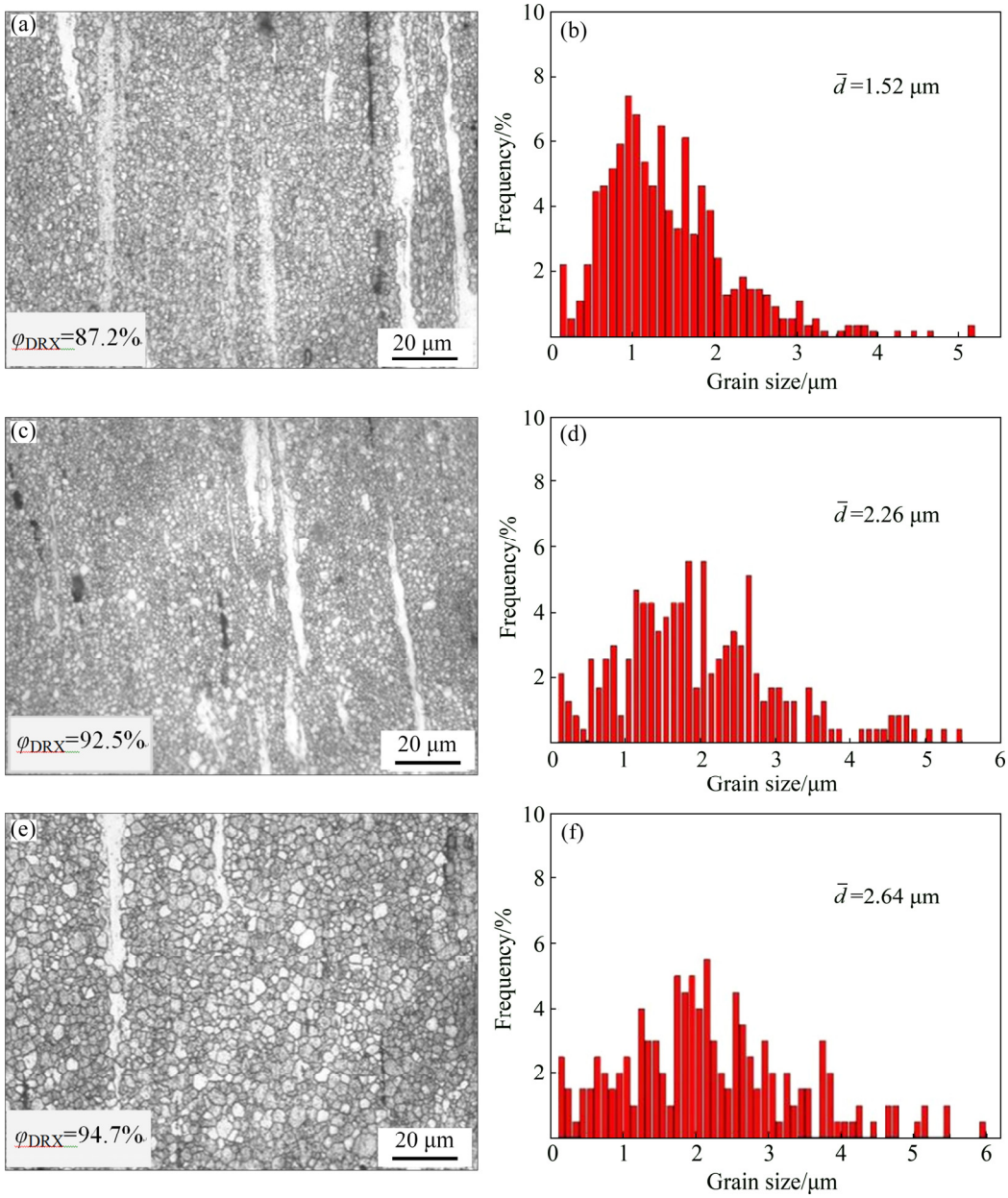


**Fig. 5** Optical micrographs (a, c, e) and average grain sizes (b, d, f) of Mg−3Zn−1Y−0.6Zr−0.5Ca alloys extruded at different temperatures ($\varphi_{DRX}$ represents volume fraction of DRX): (a, b) 270 °C; (c, d) 300 °C; (e, f) 330 °C

the extrusion temperature increases from 270 to 330 °C, the driving force for DRX and grain growth increases and the grain boundary migration ability increases. After processing by hot extrusion, there are more fine grains around the second phase, as shown in Fig. 5. In Fig. 5 white areas are the unDRXed regions, and there are almost no second phases in these areas. It is well-known that an incompatibility occurs at the interface between the soft grains of Mg matrix and hard second phases. In this way, strong stress concentration will create during the deformation, in which the formation of fine DRXed grains will be induced [28]. Besides, the second phases such as $MgZn_2$ and *I*-phases accelerated the formation of DRXed grains by inducing a stress concentration around these particles. Meanwhile, both of them play a critical role in restricting DRXed grain growth by generating a pinning effect.

Figure 6 shows the SEM images of alloys extruded at different temperatures. The EDS results in Table 2 confirm the presence of *I*-phase. It can be seen from Fig. 6 that eutectic *I*-phase of the alloys is elongated and crushed during hot extrusion. But the *I*-phase is not completely destroyed and homogeneously distributed in the magnesium matrix (Fig. 6(c)), which could help to refine the grains of the Mg matrix. Meanwhile, it can be observed that there are ultra-fine spherical precipitates from the high magnification SEM image (Fig. 6(d)). It may be classified as $MgZn_2$ according to the research by

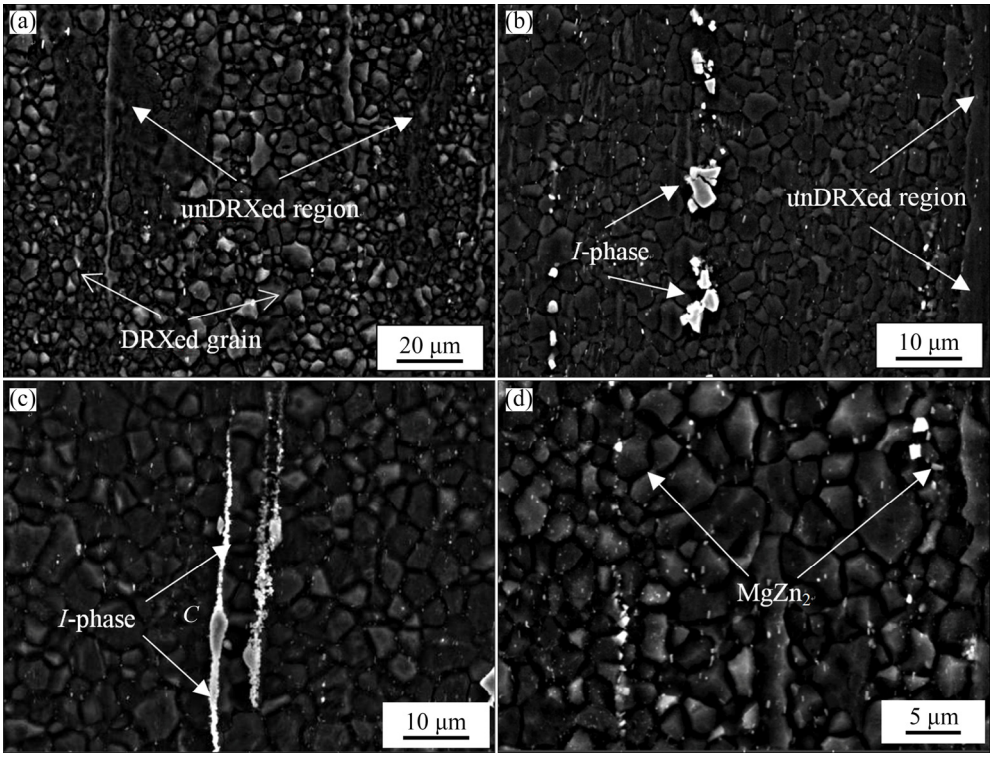


**Fig. 6** SEM images of Mg−3Zn−1Y−0.6Zr−0.5Ca alloys extruded at different temperatures: (a) 270 °C; (b) 300 °C; (c, d) 330 °C

**Table 2** EDS results of phases at Point *C* in Fig. 6(c)

| Content/at.% | | | | | Possible phase |
|---|---|---|---|---|---|
| Mg | Zn | Y | Zr | Ca | |
| 25.0 | 54.1 | 20.1 | 0.8 | − | $Mg_3YZn_6$ |

LI et al [29] and XRD results in Fig. 3. It cannot be recognized by EDS due to its small size. These precipitates distribute dispersedly within the grain interiors and at grain boundaries, which may effectively hinder the migration of grain boundaries. It was reported that *I*-phase could act as dynamic recrystallization sources during hot extrusion, thereby realizing inhibiting grain growth [30,31]. However, the number density of the second phases increases significantly when the extrusion temperature increases, as shown in Fig. 6. SUN et al [32] reported that these second phase particles can provide more nucleation sites for DRX. This is consistent with the conclusion that $\varphi_{DRX}$ increases as the extrusion temperature increases.

### 3.2 Texture of extruded alloys

In order to further elaborate microstructural evolution precisely at different extrusion temperatures, the EBSD analysis was used. Figure 7 shows the inverse pole figure (IPF) maps of the Mg−3Zn−1Y−0.6Zr−0.5Ca alloys extruded at different temperatures and corresponding misorientation angle distribution. It can be seen from Figs. 7(a, c, e) that the alloy grains grow up with the increase of extrusion temperature, which is consistent with the OM observation in Fig. 5. Moreover, different colors of the grains represent their respective orientation in IPF maps. So, it can be concluded that the fine DRXed grains show relatively random orientation. In other words, the texture intensity of the as-extruded alloy specimen is highly weak. The relatively frequent misorientation angles of alloys at different extrusion temperatures are presented in Figs. 7(b, d, f). In general, low angular grain boundaries (LAGBs) are 2°−15° and high angular grain boundaries (HAGBs) are 15°−100° [33]. It can be seen that LAGBs fraction decreases and HAGBs fraction increases gradually with the increase of extrusion temperature. Statistics from the histogram in Figs. 7(b, d, f) suggests that the fractions of LAGBs at three extrusion temperatures are 5.3%, 4.6% and 1.9%, respectively. DRX fraction is inversely proportional to the fraction of LAGBs. With the increase of temperature, recrystallization nucleation becomes easy and dislocation migration ability is enhanced. Substructures in high angular grains will be eliminated in the process of extrusion, thus resulting in the decrease of LAGBs fraction [34].

The (0001) and $(11\bar{2}0)$ pole figures, parallel to ED of Mg−3Zn−1Y−0.6Zr−0.5Ca alloy extruded at various temperatures, are shown in Fig. 8. According to the basal plane (0001) figure, the maximum texture intensities of samples extruded at extrusion temperatures of 270, 300 and 330 °C are 10.07, 9.29 and 7.19, respectively. It can be summarized that the basal plane texture tends to be

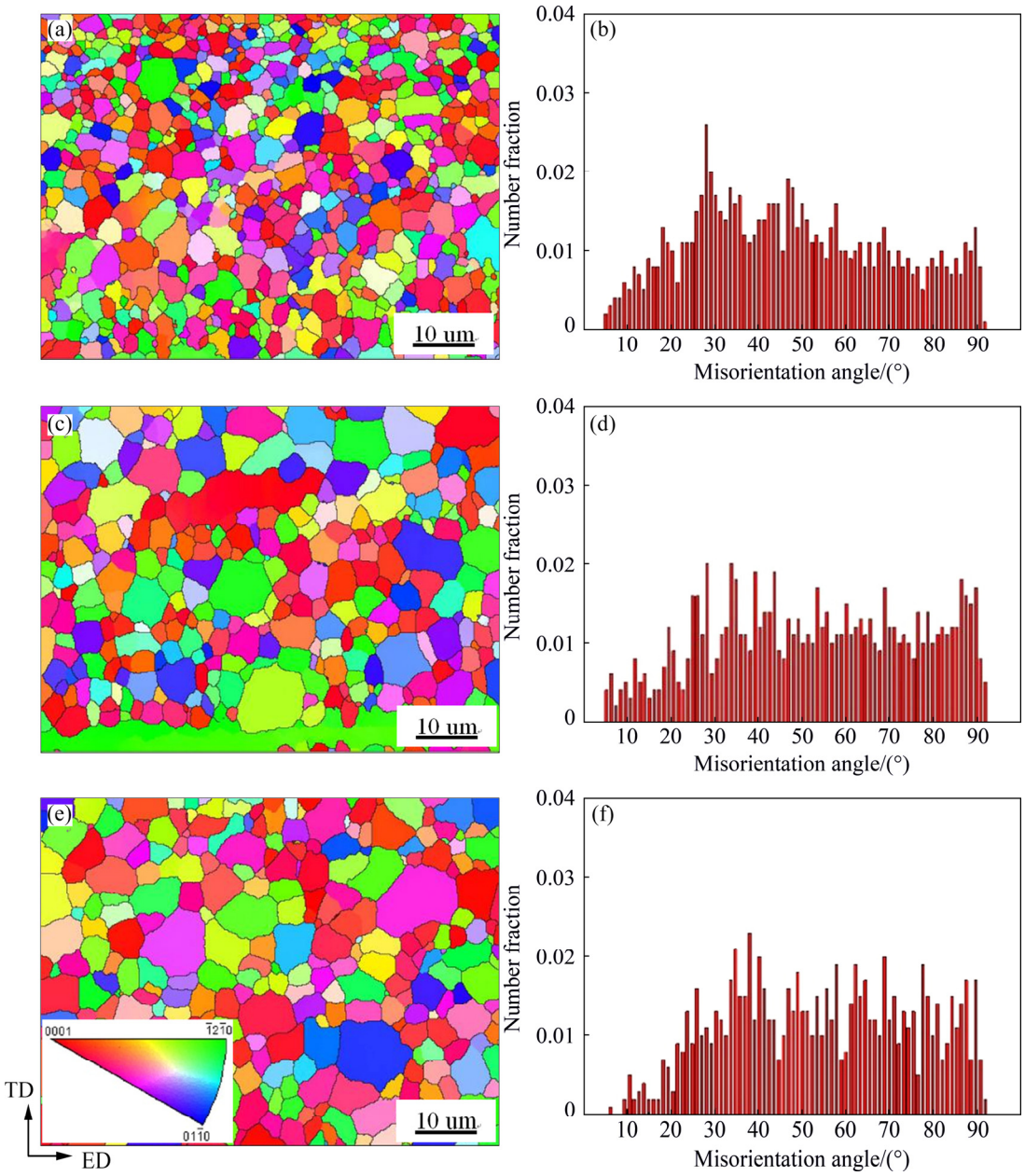


**Fig. 7** Inverse pole figure maps and misorientation angle distribution of as-extruded alloys at different temperatures (ED and TD stand for extrusion direction and transverse direction, respectively): (a, b) 270 °C; (c, d) 300 °C; (e, f) 330 °C

weak with the increase of extrusion temperature, which means that the anisotropy of the as-extruded alloys decreases. It has been already calculated from OM that the DRX volume fraction $\varphi_{DRX}$ increases when the extrusion temperature increases. In addition, the unDRX regions commonly exhibit stronger basal texture intensity than DRX regions in the extruded Mg alloys [35,36]. So, the decreasing amount of unDRXed regions with increasing extrusion temperature leads to the weakening of basal plane texture. Besides, with the extrusion temperature increasing, the critical resolved shear stress (CRSS) difference in slip systems decreases, and potential non-basal slip systems can be easily operated, which may contribute to the formation of weaker texture [37].

### 3.3 Mechanical properties and fraction behaviors

The tensile properties of the as-cast and as-extruded samples at room temperature are shown in Fig. 9. The yield strength (YS) and ultimate tensile strength (UTS) of the as-cast specimens arrive only at 85 and 192 MPa, respectively. The elongation (EL) only arrives at approximately 12%. The strength and EL of the extruded alloys are obviously higher than those of the as-cast alloy. The UTS of the alloy extruded at 270 °C reaches 315 MPa, which is higher than that of other experimental

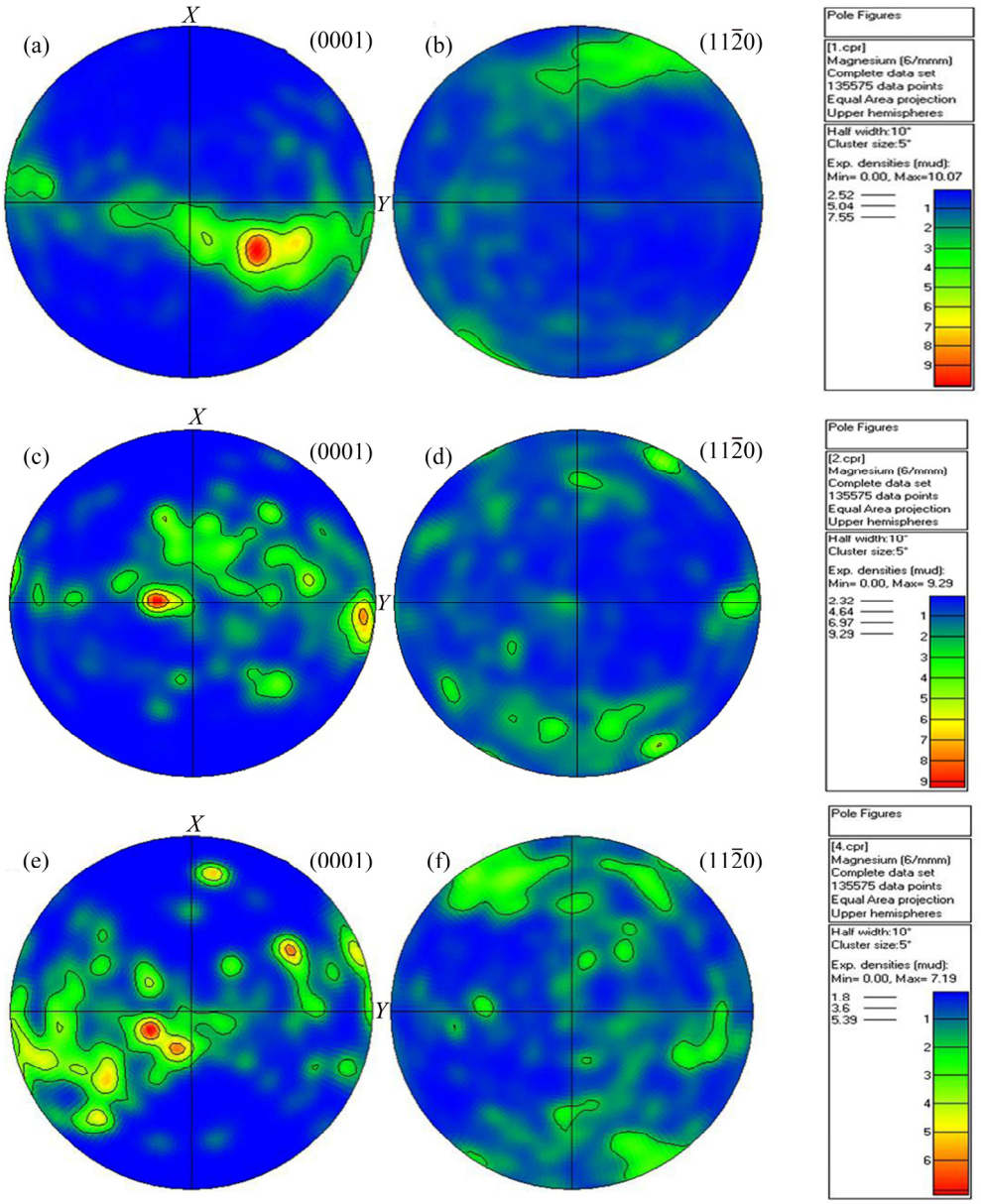


**Fig. 8** (0001) and (11$\bar{2}$0) pole figures of Mg−3Zn−1Y−0.6Zr−0.5Ca alloy extruded at different temperatures: (a, b) 270 °C; (c, b) 300 °C; (e, f) 330 °C

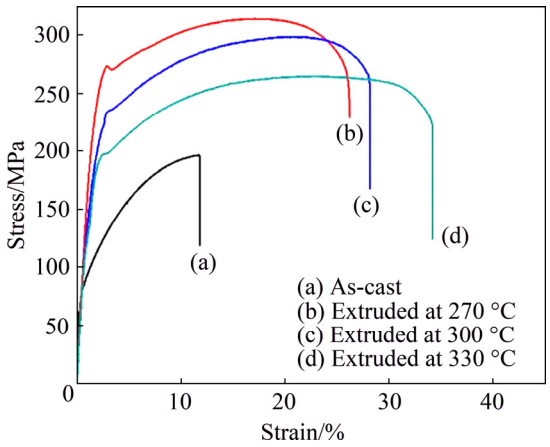


**Fig. 9** Tensile stress−strain curves of as-cast and as-extruded Mg−3Zn−1Y−0.6Zr−0.5Ca alloys at different temperatures

alloys. And the YS and EL of the alloy extruded at 270 °C arrive at 270 MPa and 26%, respectively. Besides, it should be noticed that the extruded alloys present excellent plasticity. The EL of the alloy extruded at 330 °C reaches up to 34%. The YS and UTS decrease with the increase of extrusion temperature, but the EL increases. The alloy extruded at 270 °C has better comprehensive mechanical properties.

It is known that the YS of Mg alloys mainly depends on the grain size, second phases and texture [38]. The stress−strain graphs for the extruded alloy in YS zone show different behaviors compared to that of the as-cast alloy. As we discussed above, the fine and uniform dynamic recrystallized grains are obtained during the extrusion, which is beneficial to the

improvement of the mechanical properties. According to Hall−Petch relation: $\sigma_y=\sigma_0+kd^{-1/2}$, here $\sigma_y$ is the YS, $\sigma_0$ is the material constant, $k$ is the Hall−Petch slope, and $d$ is the grain size. The YS of the extruded alloys is improved a lot due to grain boundaries strengthening compared with that of the as-cast alloy. Furthermore, the coarse intermetallic compounds in the as-cast alloy are broken because of hot extrusion. It can reduce the dislocation accumulations around the second phases to avoid the generation and propagation of the crack source, which is good for the improvement of mechanical properties.

After the as-cast alloys are extruded at different temperatures, the size of grain, distribution of second phases and the texture intensity have dramatic change. Obviously, with the increase of extrusion temperature, the grain size gradually increases, and the contribution to the yield strength decreases gradually. In addition to the effect of grain size, the formation of strong basal plane texture of the as-extruded alloy contributes to enhancing its strength along extrusion direction [29]. As mentioned in Fig. 8, the texture strength of the extruded alloys decreases with the increasing extrusion temperature. In this way, it may be another factor for the decrease of strength.

Figure 10 depicts SEM images of the tensile fracture surfaces for the as-cast alloy and as-extruded Mg−3Zn−1Y−0.6Zr−0.5Ca alloys. It is observed that failure surfaces of the as-cast alloy are mainly composed of tearing ridge and big dimples, which illustrates a feature of quasi-cleavage fracture. In contrast, the as-extruded alloys show complete ductile fracture.

It is found that a number of dimples in the extruded alloy are extensively increased on the fracture surface. Besides, many second phase particles can be observed inside small dimples marked with red circles in Fig. 10. As the extrusion temperature increases, the dimples distribute more uniformly and these dimples become larger and deeper, which leads to better ductility of alloys. Furthermore, the larger grain size and weaker texture are observed from the texture analysis in Fig. 8, both of the aspects are conductive to the dislocation accumulation and deformation coordination. Some researchers pointed out that the Ca-contained magnesium alloys have a weaker basal texture and better grain sizes for the activitation of the non-basal slip system and the formation of strong non-basal texture [39]. All these could be the reason that the ductility of the alloys is improved at higher temperatures.

Figure 11(a) gives the magnified SEM image of the tensile fracture surfaces extruded at 270 °C. The EDS result of the cracked particle marked by red cross is shown in Fig. 11(b). It indicates that Mg, Zn and Y elements are detected and the atomic ratio of Zn/Y is approximately 5:1. Therefore, the particles are demonstrated to be *I*-phase. In general, *I*-phase particles gather at the dimples and crack firstly. That is due to unmatched deformation stress between the *I*-phase and the matrix. A large number of dislocations gather around

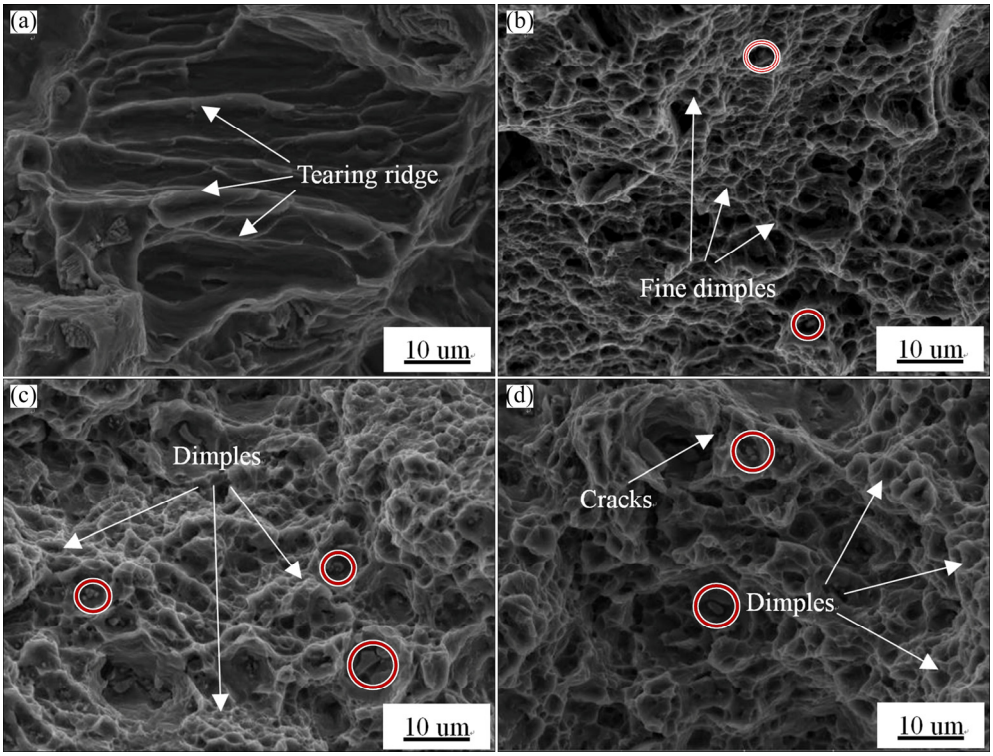


**Fig. 10** SEM images of tensile fracture surfaces for as-cast and as-extruded alloys at different temperatures: (a) As-cast; (b) 270 °C; (c) 300 °C; (d) 330 °C

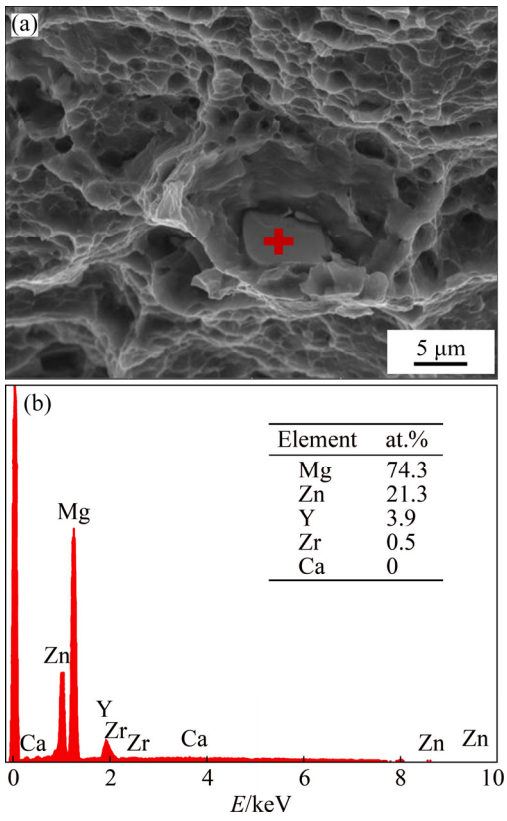


**Fig. 11** SEM image of tensile fracture surfaces extruded at 270 °C (a) and corresponding EDS results (b)

*I*-phase during deformation and induce the formation of microcracks. So, some second phases can be observed in the dimples. In addition, the second phases in the dimples have a positive impact on enhancing mechanical properties. During the tensile deformation process, the movement of dislocation can be strongly pinned and hindered by *I*-phase particles, which contributes to the strength of materials. Besides, strength increment of the precipitates is associated with the Orowan mechanism [40].

$$\Delta\sigma_{\mathrm{p}} = M\frac{Gb}{2\pi\sqrt{1-\upsilon}}\frac{1}{\bar{d}[\sqrt{\pi/(4f-1)}]}\ln\frac{\bar{d}}{b} \quad (1)$$

where $M$ is the strengthening coefficient, $G$ is the shear modulus of the alloy, $b$ is the Burger vector value, $\upsilon$ is the Possion ratio, $d$ is the size of precipitates, and $\bar{d}$ is the average size of precipitates. It can be estimated that the Orowan strengths are about 15.4, 18.8 and 19.6 MPa for the extrusion conditions of 270, 300 and 330 °C, respectively. Accordingly, increasing the amount of precipitates can improve the strength of alloys.

## 4 Conclusions

(1) The as-cast Mg−3Zn−1Y−0.6Zr−0.5Ca alloys are mainly composed of $\alpha$-Mg matrix, $MgZn_2$ phase and *I*-phase ($Mg_3YZn_6$). The *I*-phase distributes at the triangular grain boundaries, which plays an important role in performance of as-cast alloy.

(2) The compositions of the alloy do not change after hot extrusion; however, the microstructure is refined effectively and the second phases are fragmented. With the increase of extrusion temperature from 270 to 330 °C, the grain size increases gradually from 1.52 to 2.64 μm. The DRX extent is higher and the grain distribution becomes more uniform.

(3) All as-extruded samples show relatively random orientation and weak texture extremely, and the maximum texture intensity decreases with the increasing extrusion temperature owing to the increasing volume fraction of DRX.

(4) The mechanical properties of the alloys are greatly enhanced after extrusion. The UTS is decreased and the EL is improved with the increase of extrusion temperature. Besides, the optimum comprehensive mechanical properties are achieved in the Mg−3Zn−1Y−0.6Zr−0.5Ca alloy extruded at 270 °C, with the YS, UTS and EL of 270 MPa, 315 MPa and 26%, respectively. This is attributed to the effect of small grain size, pinning second phases and weak texture.

## References

[1] WITTE F, KAESE V, HAFERKAMP H, SWITZER E, MEYER-LINDENBERG A, WIRTH C J, WINDHAGEN H. In vivo corrosion of four magnesium alloys and the associated bone response [J]. Biomaterials, 2005, 26(17): 3557−3563.

[2] FRANK W, NORBERT H, CARLA V, SMADAR C, ULRICH K K, REGINE W, FRANK F. Degradable biomaterials based on magnesium corrosion [J]. Current Opinion in Solid State and Materials Science, 2008, 12(5−6): 63−72.

[3] LI Ji-lin. CHEN Rong-shi. MA Yue-qun. KE Wei. Effect of Zr modification on solidification behavior and mechanical properties of Mg−Y−RE (WE54) alloy [J]. Journal of Magnesium and Alloys, 2013, 1(4): 346−351.

[4] YUAN Guang-yin, ZHANG Xiao-bo, NIU Jia-lin, TAO Hai-rong, CHEN Dao-yun, HE Yao-hua, JIANG Yao, DING Wen-jiang. Research progress of new type of degradable biomedical magnesium alloys JDBM [J]. The Chinese Journal of Nonferrous Metals, 2011, 21(10): 2476−2488. (in Chinese)

[5] GU X N, GUO H M, WANG F, LU Y, LIN W T, LI J, ZHENG Y F, FAN Y B. Degradation, hemolysis, and cytotoxicity of silane coatings on biodegradable magnesium alloy [J]. Materials Letters, 2017, 193: 266−269.

[6] MENSAHDARKWA K, GUPTA R K, KUMAR D. Mechanical and corrosion properties of magnesium−hydroxyapatite (Mg−HA) composite thin films [J]. Journal of Materials Science & Technology, 2013, 29(9): 788−794.

[7] MERT F. Wear behaviour of hot rolled AZ31B magnesium alloy as candidate for biodegradable implant material [J]. Transactions of Nonferrous Metals Society of China, 2017, 27: 2598−2606.

[8] TONG L B, LI X, ZHANG D P, CHENG L R, MENG J, ZHANG H J. Dynamic recrystallization and texture evolution of Mg−Y−Zn alloy during hot extrusion process [J]. Materials Characterization,

2014, 92: 77−83.
[9] PARK S H, SUN Y B, MISHRA RAJA K, SACHDEV ANIL K. Effects of extrusion parameters on the microstructure and mechanical properties of Mg−Zn−(Mn)−Ce/Gd alloys [J]. Materials Science and Engineering A, 2013, 583(10): 25−35.
[10] PARK S S, YOU B S, YOON D J. Effect of the extrusion conditions on the texture and mechanical properties of indirect-extruded Mg−3Al−1Zn alloy [J]. Journal of Materials Processing Technology, 2009, 209(18): 5940−5943.
[11] ZHANG B P, GENG L, HUANG L J, ZHANG X X, DONG C C. Enhanced mechanical properties in fine-grained Mg−1.0Zn−0.5Ca alloys prepared by extrusion at different temperatures [J]. Scripta Materialia, 2010, 63(10): 1024−1027.
[12] MIRZADEH H, ROOSTAEI M, PARSA M H, MAHMUDI R. Rate controlling mechanisms during hot deformation of Mg−3Gd−1Zn magnesium alloy: Dislocation glide and climb, dynamic recrystallization, and mechanical twinning [J]. Materials & Design, 2015, 68: 228−231.
[13] HAMED M. Constitutive analysis of Mg−Al−Zn magnesium alloys during hot deformation [J]. Mechanics of Materials, 2014, 77: 80−85.
[14] DU Zhi-ming, WANG Da-yu, ZHANG Hong-juan. Influence of hot extrusion process on microstructure and mechanical properties of Mg−Zn−Y−Zr magnesium alloy [J]. Rare Metal Materials and Engineering, 2018, 47(6): 1655−1661.
[15] SUN Yu, ZHANG Bao-ping, WANG Yin, GENG Lin, JIAO Xiao-hui. Preparation and characterization of a new biomedical Mg−Zn−Ca alloy [J]. Materials & Design, 2012, 34: 58−64.
[16] HUANG Hua, TIAN Yuan, YUAN Guang-yin, CHEN Chun-lin, WANG Zhong-chang, DING Wen-jiang, INOUE A. Dislocations in icosahedral quasicrystalline phase embedded in hot-deformed Mg alloys [J]. Journal of Alloys and Compounds, 2016, 658: 483−487.
[17] LIU Yong, YUAN Guang-yin, DING Wen-jiang, LU Cheng. Deformation behavior of Mg−Zn−Gd-based alloys reinforced with quasicrystal and Laves phases at elevated temperatures [J]. Journal of Alloys and Compounds, 2007, 427: 160−165.
[18] CHAMANARA M, EBRAHIMI G R, EZATPOUR H R. Deformation behavior and processing maps of Mg−Zn−Y alloy containing *I* phase at elevated temperatures [J]. Transactions of Nonferrous Metals Society of China, 2018, 28: 629−641.
[19] BAE D H, LEE M H, KIM K T, KIM W T, KIM D H. Application of quasicrystalline particles as a strengthening phase in Mg−Zn−Y alloys [J]. Journal of Alloys and Compounds, 2002, 342: 445−450.
[20] MUHAMMAD S, LOTHAR W. Influence of extrusion parameters on microstructure and texture developments, and their effects on mechanical properties of the magnesium alloy AZ80 [J]. Materials Science and Engineering A, 2009, 506: 141−147.
[21] ZENG X Q, ZHANG Y, LU C, DING W J, WANG Y X, ZHU Y P. Precipitation behavior and mechanical properties of a Mg−Zn−Y−Zr alloy processed by thermo-mechanical treatment [J]. Journal of Alloys and Compounds, 2005, 395: 213−219.
[22] XU D K, LIU L, XU Y B, HAN E H. Effect of microstructure and texture on the mechanical properties of the as-extruded Mg−Zn−Y−Zr alloys [J]. Materials Science and Engineering A, 2007, 443: 248−256.
[23] ZENG Rong-chang, CUI Lan-yue, KE Wei. Biomedical magnesium alloys: Composition, microstructure and corrosion [J]. Acta Metallurgica Sinica, 2018, 54(9): 1215−1235.
[24] ELSAYED F R, SASAKI T T, OHKUBO T, TAKAHASHI H, XU S W, KAMADO S, HONO K. Effect of extrusion conditions on microstructure and mechanical properties of microalloyed Mg−Sn−Al−Zn alloys [J]. Materials Science and Engineering A, 2013, 588: 318−328.
[25] XU C, NAKATA T, QIAO X G, JIANG H S, SUN WT, CHI Y C, ZHENG M Y, KAMADO S. Effect of extrusion parameters on microstructure and mechanical properties of Mg−7.5Gd−2.5Y−3.5Zn−0.9Ca−0.4Zr (wt%) alloy [J]. Materials Science and Engineering A, 2017, 685: 159−167.
[26] MIAO Hong-wei, HUANG Hua, SHI Yong-juan, ZHANG Hua, PEI Jia, YUAN Guang-yin. Effects of solution treatment before extrusion on the microstructure, mechanical properties and corrosion of Mg−Zn−Gd alloy in vitro [J]. Corrosion Science, 2017, 122: 90−99.
[27] XU S W, ZHENG M Y, KAMADO S, WU K, WANG G J, LV X Y. Dynamic microstructural changes during hot extrusion and mechanical properties of a Mg−5.0Zn−0.9Y−0.16Zr (wt.%) alloy [J]. Materials Science and Engineering A, 2011, 528: 4055−4067.
[28] WANG Wan-hua, WANG Hong-xia, LIU Yi-ming, NIE Hui-hui, CHENG Wei-li. Effect of SiC nanoparticles addition on the microstructures and mechanical properties of ECAPed Mg9Al−1Si alloy [J]. Journal of Materials Research, 2017, 32(3): 615−623.
[29] LI Wei-jian, DENG Kun-kun, ZHANG Xiao, NIE Kai-bo, XU Fang-jun. Effect of ultra-slow extrusion speed on the microstructure and mechanical properties of Mg−4Zn−0.5Ca alloy [J]. Materials Science and Engineering A, 2016, 677: 367−375.
[30] PENG Jian, ZHONG Li-ping, WANG Yong-jian, LU Yun, PAN Fu-sheng. Effect of extrusion temperature on the microstructure and thermal conductivity of Mg−2.0Zn−1.0Mn−0.2Ce alloys [J]. Materials & Design, 2015, 87: 914−919.
[31] KOIKE J, KOBAYASHI T, MUKAI T, WATANABE H, SUZUKI M, MARUYAMA K, HIGASHI K. The activity of non-basal slip systems and dynamic recovery at room temperature in fine-grained AZ31B magnesium alloys [J]. Acta Materialia, 2003, 51(7): 2055−2065.
[32] SUN Hong-fei, LI Cheng-jie, FANG Wen-bin. Evolution of microstructure and mechanical properties of Mg−3.0Zn−0.2Ca−0.5Y alloy by extrusion at various temperatures [J]. Journal of Materials Processing Technology, 2016, 229: 633−640.
[33] JUDIT M, PABLO P, GERARDO G, PALOMA A. Effects of calcium, manganese and cerium-rich mischmetal additions on the mechanical properties of extruded Mg−Zn−Y alloy reinforced by quasicrystalline *I*-phase [J]. Materials Characterization, 2017, 129: 195−206.
[34] CHEN X M, LI L T, CHEN W Z, ZHANG W C, ZHANG L X, QIAO Y D, WANG E D. Fine-grained structure and recrystallization at ambient temperature for pure magnesium subjected to large cold plastic deformation [J]. Materials Science and Engineering A, 2017, 708: 351−359.
[35] LU Xing, ZHAO Guo-qun, ZHOU Ji-xue, ZHANG Cun-sheng, CHEN Liang, TANG Shou-qiu. Microstructure and mechanical properties of Mg−3.0Zn−1.0Sn−0.3Mn−0.3Ca alloy extruded at different temperatures [J]. Journal of Alloys and Compounds, 2018, 732: 257−269.
[36] CHEN Chao, CHEN Ji-hua, YAN Hong-ge, SU Bin, SONG Min, ZHU Su-qin. Dynamic precipitation, microstructure and mechanical properties of Mg−5Zn−1Mn alloy sheets prepared by high strain-rate rolling [J]. Materials & Design, 2016, 100: 58−66.
[37] DU Y Z, QIAO X G, ZHENG M Y, WU K, XU S W. Development of high-strength, low-cost wrought Mg−2.5mass%Zn alloy through micro-alloying with Ca and La [J]. Materials & Design, 2015, 85: 549−557.
[38] LI Cheng-jie, SUN Hong-fei, LI Xue-wen, ZHANG Jun-ling, FANG Wen-bin, TAN Ze-yi. Microstructure, texture and mechanical properties of Mg−3.0Zn−0.2Ca alloys fabricated by extrusion at various temperatures [J]. Journal of Alloys and Compounds, 2015, 652: 122−131.
[39] WANG Cui-ju, DENG Kun-kun, NIE Kai-bo, SHANG Shuan-jun, LIANG Wei. Competition behavior of the strengthening effects in as-extruded AZ91 matrix: Influence of preexisted $Mg_{17}Al_{12}$ phase [J]. Materials Science and Engineering A, 2016, 656: 102−110.
[40] WANG F L, BHATTACHARYYA JISHNU J, AGNEW SEAN R. Effect of precipitate shape and on Orowan strengthening of non-basal slip modes in hexagonal crystals, application to magnesium alloys [J]. Materials Science and Engineering A, 2016, 666: 114−122.

# 铸态和挤压态生物医用 Mg−Zn−Y−Zr−Ca 合金在不同温度下的显微组织与力学性能

贾庆功[1,2]，张文鑫[1,2]，孙 毅[1,2]，许春香[1,2]，张金山[1,2]，宽 军[1,2]

1. 太原理工大学 科学与工程学院，太原 030024；
2. 山西省高级镁基材料重点实验室，太原 030024

**摘 要**：对一种新型生物医用镁合金 Mg−3Zn−1Y−0.6Zr−0.5Ca 分别在 270，300 和 330 °C 下进行铸造和挤出实验。通过拉伸试验、光学显微镜、扫描电子显微镜、能量色散光谱、X 射线衍射技术、透射电子显微镜和电子背散射衍射研究铸态和不同挤出参数下挤压态合金的显微组织和力学性能。结果表明，270 °C 挤压态合金具有最佳的综合力学性能，其极限拉伸强度和伸长率分别达到 315 MPa 和 26%，这与晶粒细化、较弱的基底织构和第二相强化有关。经热挤压后，Mg−3Zn−1Y−0.6Zr−0.5Ca 合金出现大量动态再结晶。连续的 $Mg_3YZn_6$ 相带逐渐分裂成不连续的链状或点状结构，且晶粒分布更均匀。挤压态 Mg−3Zn−1Y−0.6Zr−0.5Ca 合金呈(0001)基面平行于挤出方向的弱织构特征。

**关键词**：镁合金；准晶；热挤压；动态再结晶；力学性能

**(Edited by Wei-ping CHEN)**